Applied Physics Letters

Ti- and Fe-related charge transition levels in $\beta - Ga_2O_3$

Cite as: Appl. Phys. Lett. **116**, 072101 (2020); https://doi.org/10.1063/1.5139402
Submitted: 19 November 2019 . Accepted: 04 February 2020 . Published Online: 18 February 2020

Christian Zimmermann, Ymir Kalmann Frodason, Abraham Willem Barnard, Joel Basile Varley, Klaus Irmscher, Zbigniew Galazka, Antti Karjalainen, Walter Ernst Meyer, Francois Danie Auret, and Lasse Vines

Applied Physics Letters ARTICLE scitation.org/journal/apl

Ti- and Fe-related charge transition levels in $\beta - Ga_2O_3$

Cite as: Appl. Phys. Lett. **116**, 072101 (2020); doi: 10.1063/1.5139402
Submitted: 19 November 2019 · Accepted: 4 February 2020 ·
Published Online: 18 February 2020

Christian Zimmermann,[1,a)] Ymir Kalmann Frodason,[1] Abraham Willem Barnard,[2] Joel Basile Varley,[3] Klaus Irmscher,[4] Zbigniew Galazka,[4] Antti Karjalainen,[5] Walter Ernst Meyer,[2] Francois Danie Auret,[2] and Lasse Vines[1]

AFFILIATIONS

[1]Department of Physics/Centre for Materials Science and Nanotechnology, University of Oslo, Blindern, P.O. Box 1048, Oslo N-0316, Norway
[2]Department of Physics, University of Pretoria, Lynnwood Road, Pretoria 0002, South Africa
[3]Lawrence Livermore National Laboratory, Livermore, California 94550, USA
[4]Leibniz-Institut für Kristallzüchtung, Max-Born-Straße 2, 12489 Berlin, Germany
[5]Department of Applied Physics, Aalto University, 00076 Aalto, Finland

[a)]**Electronic mail:** christian.zimmermann@fys.uio.no

ABSTRACT

Deep-level transient spectroscopy measurements on β-Ga_2O_3 crystals reveal the presence of three defect signatures labeled E_{2a}, E_{2b}, and E_3 with activation energies at around 0.66 eV, 0.73 eV, and 0.95 eV below the conduction band edge. Using secondary ion mass spectrometry, a correlation between the defect concentration associated with E_3 and the Ti concentration present in the samples was found. Particularly, it is found that E_3 is the dominant Ti-related defect in β-Ga_2O_3 and is associated with a single Ti atom. This finding is further corroborated by hybrid functional calculations that predict Ti substituting on an octahedral Ga site, denoted as Ti_{GaII}, to be a good candidate for E_3. Moreover, the deep level transient spectroscopy results show that the level previously labeled E_2 and attributed to Fe substituting on a gallium site (Fe_{Ga}) consists of two overlapping signatures labeled E_{2a} and E_{2b}. We tentatively assign E_{2a} and E_{2b} to Fe substituting for Ga on a tetrahedral or an octahedral site, respectively.

Monoclinic gallium sesquioxide (β-Ga_2O_3) has attracted considerable attention in recent years due to its wide bandgap and exceptionally high break-down electrical fields,[1] rendering it a potential candidate for applications in UV sensors and power electronics.[1–6] Defects, however, influence the optical and electrical properties of the material and need to be understood for β-Ga_2O_3 to live up to its potential. For example, defects can pin the Fermi-level in semiconductor–metal or semiconductor–insulator–metal junctions and hence influence the performance of devices for power electronics.[4,7–9]

Intentional and unintentional impurities are particularly relevant defects in β-Ga_2O_3. For example, iron (Fe) is commonly used to achieve semi-insulating β-Ga_2O_3 needed for obtaining field effect transistors based on β-Ga_2O_3,[1,6] while titanium (Ti) is often used as Ohmic contact on β-Ga_2O_3.[1,4,6,10–12] Furthermore, Ti in β-Ga_2O_3 was also proposed as a promising defect for quantum information processing.[13,14] Fe and Ti are believed to give rise to deep electronic states in β-Ga_2O_3.[15–19] Indeed, several defect-related electronic levels have been observed by deep level transient spectroscopy (DLTS). In particular, the defect levels commonly labeled as E_1, E_2, and E_3, with energy level positions at 0.56 eV, 0.78 eV, and 1.01 eV below the conduction band edge, respectively, have all been proposed to be related to impurities due to their lack of response to irradiation.[20] Indeed, E_2 has been identified as being related to Fe_{Ga} using DLTS in combination with secondary ion mass spectrometry (SIMS) and hybrid functional calculations.

In this study, we report on a combined DLTS and SIMS study. Using both techniques, we were able to tentatively identify a defect level with an activation energy of 0.95 eV below the conduction band edge to be associated with Ti substituting on an octahedral gallium (Ga) site and denoted as Ti_{GaII}. The corresponding level is commonly observed in commercially available β-Ga_2O_3 and is often labeled

as E_3. Our identification is corroborated by hybrid functional calculations. Furthermore, we were able to show that the defect signature labeled as E_2, which is commonly seen in DLTS measurements and associated with Fe_{Ga}, indeed consists of at least two defect signatures.

β-Ga_2O_3 bulk crystals grown by edge-defined film-fed growth (EFG)[21,22] and the Czochralski method (CZ)[23,24] were used for this study. The EFG crystals were purchased from *Tamura Corporation*, and the CZ crystals were obtained from the *Leibniz-Institut für Kristallzüchtung (Berlin)*. Furthermore, β-Ga_2O_3 thin-films grown by halide vapor-phase epitaxy (HVPE)[4] on conductive β-Ga_2O_3 substrates and obtained from *Novel Crystal Technology Inc.* were used as reference materials with a low impurity content. All samples were prepared for DLTS measurements, and hence, Ohmic contacts (Ti/Al or InGa eutectic alloy) and Schottky contacts (Ni or Pt) were deposited on the back and front sides, respectively. The resulting junctions exhibit a rectification of at least two orders of magnitude and a series resistance never exceeding 1 kΩ. The samples displayed donor concentrations ranging from 5×10^{15} cm^{-3} to 7×10^{18} cm^{-3}. Further details regarding the fabrication of Schottky diodes can be found in Ref. 25 for the CZ crystals and in Refs. 12, 15, and 20 for the EFG and HVPE samples.

DLTS measurements were performed on two different setups described in detail elsewhere,[20,26] with one setup covering the temperature range from 20 K to 400 K and one high-temperature setup enabling measurements between 150 K and 700 K. In short, a reverse bias of −10 V and a filling pulse of 10 V were deployed for conventional DLTS measurements, while Laplace DLTS was performed at a reverse bias of −2 V and a filling pulse of 1.8 V. Laplace DLTS measurements were analyzed with a software written by Dobaczewski *et al.*[27,28] A GS4 filter was utilized to construct the conventional DLTS spectra in order to better resolve the defect signatures E_2 and E_3,[29] and the spectra were simulated with a python-based script. Parameters such as the trap concentration N_t, the activation energy E_A, and the apparent capture cross section σ_{na} of the individual traps were obtained from Laplace DLTS measurements by constructing an Arrhenius plot,[27,30] while these parameters were extracted from conventional DLTS measurements from the afore-mentioned simulations. In both cases, the extracted value for σ_{na} can be expected to exhibit a large uncertainty. For calculating N_t, the λ-correction was included.[25,30]

SIMS measurements were performed using a Cameca IMS 7f instrument with a primary beam of 10 ke V O_2^+ ions. For Ti, the absolute concentration was determined using an implanted reference sample. Crater depths were measured using a Dektak Stylus Profilometer to convert sputtering time to depth.

First-principles calculations were performed using the projector augmented wave method[31,32] and the Heyd–Scuseria–Ernzerhof (HSE)[33] screened hybrid functional, as implemented in the VASP code.[34] The fraction of screened Hartree–Fock exchange was adjusted to $\alpha = 0.33$, resulting in a direct bandgap of 4.9 eV.[35] The experimentally determined bandgap value can be expected to exhibit an uncertainty of around ± 0.1 eV.[35] The Ga-3*d* and Ti-3*p*, -3*d*, and -4*s* electrons were included as valence states. For defect calculations, we used 160-atom supercells, a plane wave energy cutoff of 500 eV, and a single special *k*-point at (1/4, 1/4, 1/4). Defect formation energies and thermodynamic charge-state transition levels were calculated by following the well-established formalism.[36] For charged defects, we adopted the anisotropic[37] Freysoldt, Neugebauer, and Van de Walle scheme to correct formation energies[38] and the method recently proposed by Gake *et al.* to correct vertical transition energies.[39] Nonradiative carrier capture barriers were estimated by using the one-dimensional configuration coordinate (CC) model.[40] The CC diagrams were derived from the calculated one-dimensional CC model parameters by using a harmonic approximation.[41]

Figure 1(a) shows DLTS spectra recorded on an EFG-grown β-Ga_2O_3 crystal. Three defect signatures are observed labeled as E_{2a} ($E_A = 0.66$ eV, $\sigma_{na} = 4 \times 10^{-16}$ cm^2), E_{2b} ($E_A = 0.73$ eV, $\sigma_{na} = 1 \times 10^{-15}$ cm^2), and E_3 ($E_A = 0.95$ eV, $\sigma_{na} = 4 \times 10^{-14}$ cm^2). Defect signatures similar to E_{2a} and E_{2b} were found in EFG- and CZ-grown β-Ga_2O_3 crystals and HVPE-grown β-Ga_2O_3 thin-films, while E_3 was only found in EFG- and CZ-grown β-Ga_2O_3 crystals. Notably, on similar samples, the E_A values of around 1.04 eV (Ref. 25) and 1.01 eV (Ref. 20) have been reported previously for E_3. Hence, an uncertainty of around 0.1 eV can be assumed for the values of E_A stated here. Considering the previously reported values for σ_{na} of E_2 and E_3,[20,25] an uncertainty of around +/− an order of magnitude can be expected.

Figure 1(b) displays the results obtained performing Laplace DLTS on an EFG-grown β-Ga_2O_3 crystal. The corresponding results corroborate the findings presented above and in Fig. 1(a). Three defect signatures were revealed: E_{2a} ($E_A = 0.56$ eV, $\sigma_{na} = 1 \times 10^{-17}$ cm^2), E_{2b} ($E_A = 0.70$ eV, $\sigma_{na} = 4 \times 10^{-16}$ cm^2), and E_3 ($E_A = 0.98$ eV, $\sigma_{na} = 4 \times 10^{-14}$ cm^2). These parameters match well with the results obtained from simulations of conventional DLTS spectra. The defect parameters extracted from conventional and Laplace DLTS measurements are summarized in Table I.

In previous studies, the signatures E_{2a} and E_{2b} were observed as a single defect signature labeled E_2,[9,15,25,42,43] which was attributed to Fe_{Ga}.[15] E_2 and E_3 are present in a variety of commercially available β-Ga_2O_3 crystals and thin-films.[9,15,25,42–46] Notably, neither E_2 nor E_3 has been found to be affected by irradiation with protons,[15,20]

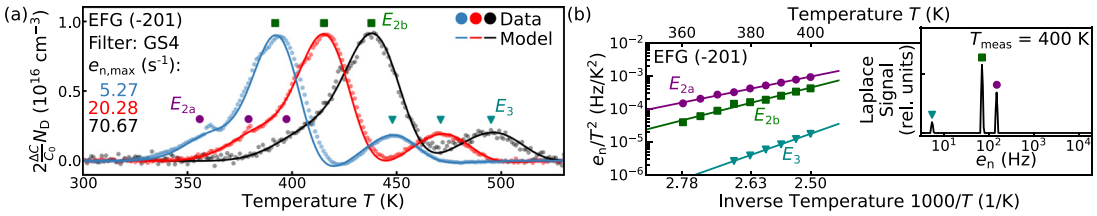

FIG. 1. (a) DLTS spectra recorded on an EFG-grown β-Ga_2O_3 crystal. The data were modeled with a simulation, and three defect signatures labeled as E_{2a}, E_{2b}, and E_3 were unveiled. (b) Results from Laplace DLTS performed on an EFG-grown β-Ga_2O_3 crystal. The Arrhenius plot for the three defect signatures, which are also detected in (a), is shown. The inset shows the emission rate spectrum obtained from the capacitance transient recorded at 400 K.

TABLE I. Overview of the parameters determined for defect signatures observed in a variety of β-Ga_2O_3 crystals. The results were obtained on EFG-, CZ-, and HVPE-grown Ga_2O_3 simulating their conventional DLTS spectra. The results in brackets were derived from Laplace DLTS measurements on an EFG-grown β-Ga_2O_3 crystal.

Defect signature	Activation energy E_A (eV)	Apparent capture cross section σ_{na} (cm^2)
E_{2a}	0.66 (0.56)	4×10^{-16} (1×10^{-17})
E_{2b}	0.73 (0.70)	1×10^{-15} (4×10^{-16})
E_3	0.95 (0.98)	4×10^{-14} (4×10^{-14})

suggesting the involvement of an impurity. After irradiation with protons or α-particles, another level commonly labeled as E_2^* with a charge transition level of around 0.75 eV below the conduction band edge is present in the same temperature region in DLTS measurements.[15,20,43,47] E_2^*, however, displays a significantly different activation energy and an apparent capture cross section compared to, for example, E_{2a}, suggesting a different origin. Moreover, the trap concentrations associated with E_{2a} and E_{2b} exhibit a ratio of approximately 1:5 (not shown). Notably, a similar ratio is expected for the two configurations of Fe_{Ga}, assuming a difference in the formation energy of 0.3 eV (Ref. 15) at the melting point temperature.[48,49] Notably, an electron paramagnetic resonance (EPR) study also found a ratio of 1:5 for the two different crystallographic configurations of Fe_{Ga} in β-Ga_2O_3.[50] Hence, we suggest that E_{2a} and E_{2b} arise from the tetrahedral and octahedral configuration of Fe_{Ga}, respectively.

Figure 2(a) shows an overview over DLTS spectra recorded on a variety of Schottky junctions including CZ-, EFG- and HVPE-grown β-Ga_2O_3. The trap concentration in HVPE-grown β-Ga_2O_3 is generally significantly lower than in CZ- or EFG-grown β-Ga_2O_3 as reported earlier.[20] For some CZ-grown β-Ga_2O_3 crystals [see CZ A in Fig. 2(a)], it was not possible to model the region where E_{2a} and E_{2b} are present with only two defect signatures, indicating the presence of additional defect signatures in this temperature region in DLTS measurements. The modeling of conventional DLTS spectra described the signature related to E_3, suggesting that, indeed, only one defect contributes to this defect signature, as corroborated by Laplace DLTS [see Fig. 1(b)].

A wide range of concentrations associated with E_{2a}, E_{2b}, and E_3 are found in CZ- and EFG-grown samples as reported previously,[15,25] rendering them suitable candidates for the identification of impurity-related defects. SIMS measurements reveal that Ti, Fe, Mg, Al, and Si are present in at least some of the investigated samples. In addition to the correlation between E_2 and Fe reported previously,[15] the concentration of E_3 was found to correlate solely with that of Ti. Figure 2(b) displays the correlation between the Ti concentration [Ti] as determined by SIMS and the E_3 trap concentration [E_3] as determined by DLTS (square brackets denote concentration). A linear relationship between [Ti] and [E_3] can be seen. Notably, all data points fall close to the line expected for [Ti] = [E_3], suggesting that E_3 is the dominant Ti-related trap and associated with a single Ti atom. Importantly, in HVPE-grown β-Ga_2O_3, the concentration of both Ti and E_3 was found to be below the detection limit of our systems, further corroborating the correlation between Ti and E_3.

To gain insights into the formation of defects involving Ti in β-Ga_2O_3 and corroborate the observed correlation between [E_3] and [Ti], we have performed hybrid functional calculations. Only results for the Ti_{Ga} configurations are presented since Ti_O and Ti_i configurations were found to have significantly higher formation energies (not shown). Figure 3(a) displays the formation energy diagram for Ti_{GaI} and Ti_{GaII}, where GaI and GaII denote the tetrahedral and octahedral Ga sites in the β-Ga_2O_3 lattice. Ti_{GaII} has the lowest formation energy regardless of the Fermi level position: the difference is 0.34 eV and 0.86 eV for the positive and neutral charge states, respectively. This means that Ti_{GaII} is expected to be the dominant configuration for Ti_{Ga}, which is consistent with EPR studies performed on β-Ga_2O_3 crystals, where only Ti_{GaII} was identified.[13,14,16] A recent study reporting first-principles calculations on Ti in β-Ga_2O_3 found very similar results for Ti_{Ga}.[19] Furthermore, the solubility of Ti is expected to be around 1.5 at. % in β-Ga_2O_3,[51] which is consistent with the low formation energy found here for Ti_{GaII}. Notably, the amount of unintentionally incorporated Ti will strongly depend on both the amount of Ti present and the experimental conditions during growth.

Ti_{Ga} is predicted to act as a deep single donor on both lattice sites. In the neutral charge state, the donor electron occupies a localized defect state within the bandgap, showing mainly Ti 3*d* character. The calculated thermodynamic (+/0) charge state transition level of Ti_{GaI} and Ti_{GaII} occurs at 0.60 eV and 1.13 eV below the conduction band minimum (CBM), respectively. To enable a more direct comparison with the DLTS results, we have estimated the classical capture barrier for electrons E_b by constructing a CC diagram,[40] as shown in Fig. 3(b). The excited state potential energy surface corresponds to the ionized

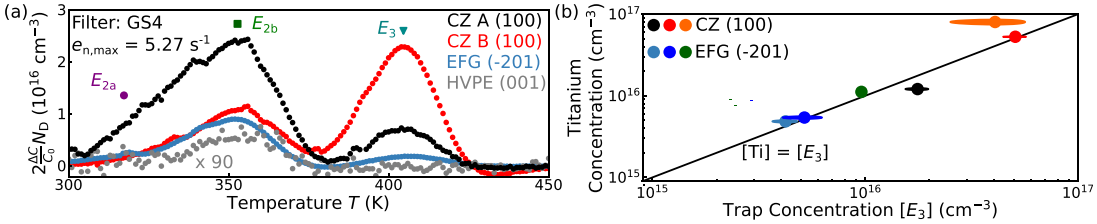

FIG. 2. (a) DLTS spectra recorded on various CZ-, EFG, and HVPE-grown β-Ga_2O_3. The corresponding surface orientations are also shown in the legend. The spectra were aligned along the temperature axis with respect to the peak position of the signature labeled E_3 as observed in the sample labeled CZ A (100). The temperature positions of E_{2a}, E_{2b}, and E_3 are marked. (b) Comparison between the titanium concentration obtained from calibrated SIMS measurements and the trap concentration related to E_3 determined by simulating conventional DLTS spectra. Ellipsoidal areas are shown if the uncertainties for [E_3] are larger than the data points displayed. The detection limit for [Ti] as measured by SIMS is estimated to be around 1×10^{15} cm^3. [Ti] in HVPE-grown β-Ga_2O_3 is below that limit, and no signal corresponding to E_3 was detected in HVPE-grown β-Ga_2O_3. As a guide, a line corresponding to [E_3] = [Ti] is shown.

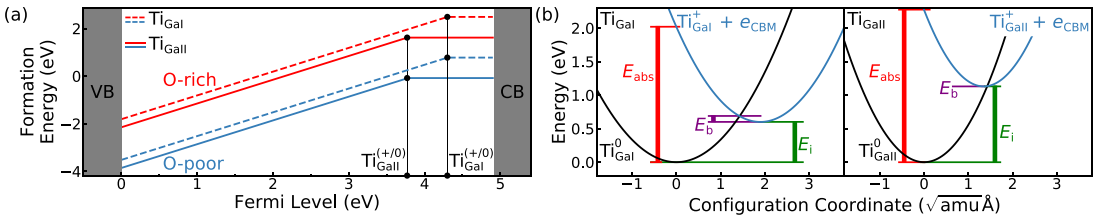

FIG. 3. (a) Formation energy of Ti_{GaI} and Ti_{GaII} in dependence of the Fermi level position. The valence and conduction band positions are marked in gray. Formation energies are displayed for O-rich and O-poor conditions. Ti_{GaII} is generally more favorable to form compared to Ti_{GaI}. Ti_{GaI} and Ti_{GaII} are deep single donors and exhibit a charge state transition from + to 0 inside the bandgap of β-Ga_2O_3 at around 0.60 eV and 1.13 eV below the conduction band edge, respectively. The corresponding transition point is marked with a black dot. (b) Configuration coordinate diagrams describing electron capture and emission between the conduction band minimum (CBM) and Ti_{Ga}. The thermal ionization energy E_i is the thermodynamic (+/0) charge transition level relative to the CBM. The absorption energy E_{abs} is related to the photon energy where the onset of optical absorption is expected within the Franck–Condon approximation. The barrier E_b for the capture of electrons is given by the crossing point between the ground and excited state potential energy surfaces.

donor plus an electron at the CBM ($Ti_{GaII}^{+} + e_{CBM}$), and the ground-state curve corresponds to the charge-neutral donor (Ti_{GaII}^{0}). The two curves are vertically displaced by the thermal ionization energy E_i, i.e., the Fermi level position of the thermodynamic (+/0) charge-state transition level relative to the CBM. In this classical picture, the activation energy for electron emission corresponds to the sum of E_i an E_b, which is taken as the energy required to reach the crossing point between the two potential energy curves. For Ti_{GaI}, we obtain a capture barrier of 0.09 eV, whereas no barrier was found for Ti_{GaII}. Note that the activation energy will be lower if its temperature-dependence is taken into account.[40] Thus, we arrive at 0.69 eV and 1.13 eV as the upper limit for the activation energy of Ti_{GaI} and Ti_{GaII}, respectively. Hence, the calculated transition level for $Ti_{GaII}^{(+/0)}$ agrees within the errors of experiment and theoretical calculation with the activation energy found for E_3 (0.95 eV), further strengthening the assignment of E_3 to Ti. The calculated defect parameters for Ti_{Ga} are summarized in Table II.

In summary, conventional DLTS measurements on selected EFG- and CZ-grown β-Ga_2O_3 crystals reveal the presence of three defect signatures labeled E_{2a}, E_{2b}, and E_3 with activation energies of around 0.66 eV, 0.73 eV, and 0.95 eV below the conduction band edge. E_{2a} and E_{2b} are also found in HVPE-grown β-Ga_2O_3 thin-films, while E_3 was not detected in such samples. It is found that the defect level labeled E_2, which is attributed to Fe_{Ga}, consists of two distinct defect signatures labeled E_{2a} and E_{2b}. It is proposed that E_{2a} and E_{2b} are associated with Fe substituting for Ga on a tetrahedral or an octahedral site, respectively. The defect concentration associated with E_3 is found to be correlated with the Ti concentration present in the samples as measured by SIMS. Particularly, it is shown that E_3 is the dominant Ti-related defect in β-Ga_2O_3 and is associated with a single Ti atom. This is further supported by hybrid functional calculations where Ti substituting on an octahedral Ga site denoted as Ti_{GaII} is shown to be an excellent candidate for E_3.

TABLE II. Summary of the parameters for Ti_{Ga} defects obtained from hybrid functional calculations. The parameters are defined as displayed in Fig. 3(b).

Defect	E_{abs} (eV)	E_i (eV)	E_b (meV)
Ti_{GaI}	2.02	0.60	86
Ti_{GaII}	2.27	1.13	3

Financial support from the Research Council of Norway through the FUNDAMENT project (Project No. 251131), the Norwegian Micro- and Nano-Fabrication Facility (NorFab, Project No. 245963), the Faculty of Mathematics and Natural Sciences at the University of Oslo via the strategic research initiative FOXHOUND, and the Norwegian nano-network is acknowledged. This work was partially performed under the auspices of the U.S. DOE by Lawrence Livermore National Laboratory under Contract No. DE-AC52-07NA27344 and partially supported by the Critical Materials Institute funded by the U.S. DOE, Office of Energy Efficiency and Renewable Energy, Advanced Manufacturing Office.

REFERENCES

[1]M. Higashiwaki, K. Sasaki, H. Murakami, Y. Kumagai, A. Koukitu, A. Kuramata, T. Masui, and S. Yamakoshi, Semicond. Sci. Technol. **31**, 034001 (2016).
[2]S. Nakagomi, T. Momo, S. Takahashi, and Y. Kokubun, Appl. Phys. Lett. **103**, 072105 (2013).
[3]S. Nakagomi, T. Sato, Y. Takahashi, and Y. Kokubun, Sens. Actuators, A **232**, 208 (2015).
[4]M. A. Mastro, A. Kuramata, J. Calkins, J. Kim, F. Ren, and S. Pearton, ECS J. Solid State Sci. Technol. **6**, P356 (2017).
[5]Z. Galazka, Semicond. Sci. Technol. **33**, 113001 (2018).
[6]S. Pearton, J. Yang, P. H. Cary IV, F. Ren, J. Kim, M. J. Tadjer, and M. A. Mastro, Appl. Phys. Rev. **5**, 011301 (2018).
[7]S. Ahn, Y.-H. Lin, F. Ren, S. Oh, Y. Jung, G. Yang, J. Kim, M. A. Mastro, J. K. Hite, C. R. Eddy, Jr. *et al.*, J. Vac. Sci. Technol., B **34**, 041213 (2016).
[8]J. F. McGlone, Z. Xia, C. Joishi, S. Lodha, S. Rajan, S. Ringel, and A. R. Arehart, Appl. Phys. Lett. **115**, 153501 (2019).
[9]J. F. McGlone, Z. Xia, Y. Zhang, C. Joishi, S. Lodha, S. Rajan, S. A. Ringel, and A. R. Arehart, IEEE Electron Device Lett. **39**, 1042 (2018).
[10]M.-H. Lee and R. L. Peterson, APL Mater. **7**, 022524 (2019).
[11]M.-H. Lee and R. L. Peterson, ECS J. Solid State Sci. Technol. **8**, Q3176 (2019).
[12]M. E. Ingebrigtsen, L. Vines, G. Alfieri, A. Mihaila, U. Badstübner, B. G. Svensson, and A. Kuznetsov, Mater. Sci. Forum **897**, 755 (2017).
[13]F. Mentink-Vigier, L. Binet, G. Vignoles, D. Gourier, and H. Vezin, Phys. Rev. B **82**, 184414 (2010).
[14]F. Mentink-Vigier, L. Binet, D. Gourier, and H. Vezin, J. Phys.: Condens. Matter **25**, 316002 (2013).
[15]M. E. Ingebrigtsen, J. Varley, A. Y. Kuznetsov, B. G. Svensson, G. Alfieri, A. Mihaila, U. Badstübner, and L. Vines, Appl. Phys. Lett. **112**, 042104 (2018).

[16]L. Binet, D. Gourier, and C. Minot, J. Solid State Chem. **113**, 420 (1994).
[17]Y. Tomm, J. Ko, A. Yoshikawa, and T. Fukuda, Sol. Energy Mater. Sol. Cells **66**, 369 (2001).
[18]C. Tang, J. Sun, N. Lin, Z. Jia, W. Mu, X. Tao, and X. Zhao, RSC Adv. **6**, 78322 (2016).
[19]M. Saleh, J. B. Varley, J. Jesenovec, A. Bhattacharyya, S. Krishnamoorthy, S. Swain, and K. Lynn, "Degenerate doping in β-Ga_2O_3 single crystals through Hf-doping," preprint arXiv:2001.11187 (2020).
[20]M. Ingebrigtsen, A. Y. Kuznetsov, B. Svensson, G. Alfieri, A. Mihaila, U. Badstübner, A. Perron, L. Vines, and J. Varley, APL Mater. **7**, 022510 (2019).
[21]H. Aida, K. Nishiguchi, H. Takeda, N. Aota, K. Sunakawa, and Y. Yaguchi, Jpn. J. Appl. Phys., Part 1 **47**, 8506 (2008).
[22]A. Kuramata, K. Koshi, S. Watanabe, Y. Yamaoka, T. Masui, and S. Yamakoshi, Jpn. J. Appl. Phys., Part 1 **55**, 1202A2 (2016).
[23]Z. Galazka, K. Irmscher, R. Uecker, R. Bertram, M. Pietsch, A. Kwasniewski, M. Naumann, T. Schulz, R. Schewski, D. Klimm *et al.*, J. Cryst. Growth **404**, 184 (2014).
[24]Z. Galazka, R. Uecker, D. Klimm, K. Irmscher, M. Naumann, M. Pietsch, A. Kwasniewski, R. Bertram, S. Ganschow, and M. Bickermann, ECS J. Solid State Sci. Technol. **6**, Q3007 (2017).
[25]K. Irmscher, Z. Galazka, M. Pietsch, R. Uecker, and R. Fornari, J. Appl. Phys. **110**, 063720 (2011).
[26]B. Svensson, K.-H. Rydén, and B. Lewerentz, J. Appl. Phys. **66**, 1699 (1989).
[27]L. Dobaczewski, P. Kaczor, I. D. Hawkins, and A. R. Peaker, J. Appl. Phys. **76**, 194 (1994).
[28]See http://info.ifpan.edu.pl/Dodatki/WordPress/laplacedlts/ for "Software Laplace Deep-Level Transient Spectroscopy 2019" (last accessed October 07, 2019).
[29]A. A. Istratov, J. Appl. Phys. **82**, 2965 (1997).
[30]P. Blood and J. Orton, *The Electrical Characterization of Semiconductors: Majority Carriers and Electron States* (Academic Press, 1992).
[31]P. E. Blöchl, Phys. Rev. B **50**, 17953 (1994).
[32]G. Kresse and D. Joubert, Phys. Rev. B **59**, 1758 (1999).
[33]A. V. Krukau, O. A. Vydrov, A. F. Izmaylov, and G. E. Scuseria, J. Chem. Phys. **125**, 224106 (2006).
[34]G. Kresse and J. Furthmüller, Phys. Rev. B **54**, 11169 (1996).
[35]C. Janowitz, V. Scherer, M. Mohamed, A. Krapf, H. Dwelk, R. Manzke, Z. Galazka, R. Uecker, K. Irmscher, R. Fornari *et al.*, New J. Phys. **13**, 085014 (2011).
[36]C. Freysoldt, B. Grabowski, T. Hickel, J. Neugebauer, G. Kresse, A. Janotti, and C. G. Van de Walle, Rev. Mod. Phys. **86**, 253 (2014).
[37]Y. Kumagai and F. Oba, Phys. Rev. B **89**, 195205 (2014).
[38]C. Freysoldt, J. Neugebauer, and C. G. Van de Walle, Phys. Rev. Lett. **102**, 016402 (2009).
[39]T. Gake, Y. Kumagai, and F. Oba, arXiv:1907.02380 (2019).
[40]D. Wickramaratne, C. E. Dreyer, B. Monserrat, J.-X. Shen, J. L. Lyons, A. Alkauskas, and C. G. Van de Walle, Appl. Phys. Lett. **113**, 192106 (2018).
[41]A. Alkauskas, Q. Yan, and C. G. Van de Walle, Phys. Rev. B **90**, 075202 (2014).
[42]A. Polyakov, N. Smirnov, I. Shchemerov, D. Gogova, S. Tarelkin, and S. Pearton, J. Appl. Phys. **123**, 115702 (2018).
[43]A. Polyakov, N. Smirnov, I. Shchemerov, E. Yakimov, J. Yang, F. Ren, G. Yang, J. Kim, A. Kuramata, and S. Pearton, Appl. Phys. Lett. **112**, 032107 (2018).
[44]A. Polyakov, N. Smirnov, I. Shchemerov, E. Yakimov, S. Pearton, C. Fares, J. Yang, F. Ren, J. Kim, P. Lagov *et al.*, Appl. Phys. Lett. **113**, 092102 (2018).
[45]Z. Zhang, E. Farzana, A. Arehart, and S. Ringel, Appl. Phys. Lett. **108**, 052105 (2016).
[46]E. Farzana, E. Ahmadi, J. S. Speck, A. R. Arehart, and S. A. Ringel, J. Appl. Phys. **123**, 161410 (2018).
[47]A. Polyakov, N. Smirnov, I. Shchemerov, S. Pearton, F. Ren, A. Chernykh, P. Lagov, and T. V. Kulevoy, APL Mater. **6**, 096102 (2018).
[48]K. Hoshikawa, E. Ohba, T. Kobayashi, J. Yanagisawa, C. Miyagawa, and Y. Nakamura, J. Cryst. Growth **447**, 36 (2016).
[49]Z. Galazka, R. Uecker, K. Irmscher, M. Albrecht, D. Klimm, M. Pietsch, M. Brützam, R. Bertram, S. Ganschow, and R. Fornari, Cryst. Res. Technol. **45**, 1229 (2010).
[50]R. Büscher and G. Lehmann, Z. Naturforsch. A **42**, 67 (1987).
[51]S. Manandhar and C. V. Ramana, Appl. Phys. Lett. **110**, 061902 (2017).